

Electronic structure and spin polarization of the Fe(001)- $p(1 \times 1)$ O surfaceA. Tange,¹ C. L. Gao,¹ B. Yu. Yavorsky,² I. V. Maznichenko,² C. Etz,¹ A. Ernst,¹ W. Hergert,² I. Mertig,^{1,2} W. Wulfhchel,^{1,3} and J. Kirschner¹¹Max-Planck-Institut für Mikrostrukturphysik, Weinberg 2, D-06120 Halle, Germany²Institut für Physik, Martin-Luther-Universität Halle-Wittenberg, D-06099 Halle, Germany³Physikalisches Institut, Karlsruher Institut für Technologie (KIT), Wolfgang-Gaede-Straße 1, 76131 Karlsruhe, Germany

(Received 23 November 2009; revised manuscript received 9 February 2010; published 6 May 2010)

We present a combined experimental and theoretical study on electronic and magnetic properties of the Fe(001)- $p(1 \times 1)$ O surface. The ordered $p(1 \times 1)$ surface is investigated with spin-polarized scanning tunneling microscopy and spectroscopy accompanied by first-principles calculations. The atomic registry of the Fe(001)- $p(1 \times 1)$ O surface was confirmed in real space from the atomically resolved images. Tunneling spectroscopy reveals two oxygen induced features in the local density of states, around -0.7 eV and at the Fermi level, the origin of which is discussed based on first-principles calculations. Due to the hybridization of oxygen p_z states with the Fe states near the Fermi level, the spin polarization in tunneling experiments is inverted upon oxygen adsorption.

DOI: [10.1103/PhysRevB.81.195410](https://doi.org/10.1103/PhysRevB.81.195410)

PACS number(s): 73.20.At, 68.37.Ef, 71.15.Mb

I. INTRODUCTION

It is generally accepted that magnetism is enhanced at surfaces of magnetic crystals, thin films, and clusters due to a reduced atomic coordination. These surfaces are, however, exposed to the surrounding environment. The adsorption of foreign atoms onto the surfaces of metals often leads to modifications of the electronic structure at the surface. While in many cases the adsorbed atoms are unwelcome, adsorption in a controlled fashion may be used to specifically tailor the structural and magnetic properties of the surface. The effects reported in the case of gaseous adsorption on iron surfaces range from an enhancement of the magnetic moments of the surface Fe atoms to an induced magnetic moment on the otherwise nonmagnetic adsorbates.¹⁻⁴ To investigate the effect of adsorption on surface magnetism, it is essential to use techniques that are sensitive to the electron spin polarization and, in particular, operate at the surface region. Spin-polarized scanning tunneling microscopy (Sp-STM) and scanning tunneling spectroscopy (STS) meet this criterion. STS has the advantage over photoemission and inverse photoemission that it is a local technique and a single experiment can reveal both occupied and unoccupied states simultaneously at the same spatial position.

Oxygen adsorption onto the iron surfaces results in different structures. So far, emphasis was made on the Fe(001)- $p(1 \times 1)$ O surface, i.e., an ordered monolayer of O on the Fe(001), because of its enhanced spin polarization.^{5,6} Both this enhancement and its relatively high stability make this surface a better candidate for spin detectors as shown recently by Winkelmann *et al.*⁷ In a recently published study, Donati *et al.* presented a non-spin-polarized STM topographical analysis of the Fe(001)- $p(1 \times 1)$ O surface.⁸ In their measurements, the crystalline structure of the surface was determined, but the observed spots were not clearly identified.

In this paper, we use a Sp-STM to confirm the atomic registry and spin density of the Fe(001)- $p(1 \times 1)$ O surface in real space. The surface structure is consistent with that from

previous dynamical low-energy electron diffraction (LEED) measurements.^{9,10} In addition, we have studied the local density of states (LDOS) and its spin polarization close to the Fermi level using STS and Sp-STM. The LDOS shows significant changes compared to the clean Fe(001) surface which is further supported by *ab initio* calculations of the electronic structure.

II. METHODS

The experiments were performed in an ultrahigh vacuum (UHV) chamber (base pressure less than 2×10^{-10} mbar) equipped with an Auger electron spectrometer (AES), a LEED, and a spin-polarized STM. The Sp-STM operates in the differential magnetic imaging mode¹¹ and uses a ferromagnetic ring as the probe electrode.¹² As STM electrodes, rings of soft magnetic material were used. The magnetization of these rings was reversed at a high frequency (20 kHz) using a small coil wound around the ring. In this way, the bottom of the ring, from which electrons can tunnel between the ring electrode and the sample, is magnetized in the surface plane and the ring plane, such that the in-plane component of the surface spin polarization is measured. For details of tip preparation and operation parameters, see Ref. 12. The variations in the tunneling current due to reversal of the ring magnetization were detected with a lock-in and are directly proportional to the sample spin polarization projected onto the direction of sensitivity of the ring electrode. Details of the construction and operation of the Sp-STM can be found elsewhere.¹³ All STM, LEED and AES measurements were performed at room temperature. Iron whiskers were used as the starting substrate. They show less defects and larger terraces compared to iron crystals grown from the melt and display a simple magnetic domain structure. The whiskers were cleaned by several cycles of 2 keV Ar⁺ bombardment and subsequent annealing to about 750 K until no contaminants could be detected by AES and no reconstructions were observed in the LEED pattern. After this process, the Fe(001) surface presents terraces several hundred nanometers wide

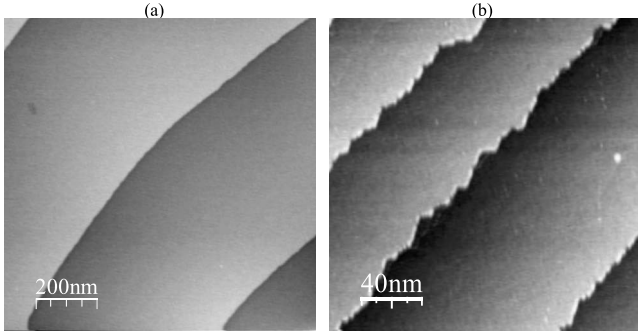


FIG. 1. STM topography of (a) clean iron whisker after repeated cycles of Ar^+ bombardment and annealing and (b) $\text{Fe}(001)-p(1 \times 1)\text{O}$ surface. Measurement parameters were $I=0.3$ nA and $U_{\text{gap}}=0.5$ V.

separated by monatomic steps [see Fig. 1(a)]. The clean $\text{Fe}(001)$ surface was exposed to oxygen at room temperature by letting in oxygen gas (99.999% pure) into the chamber through a leak valve. The oxygen exposure is given in units of langmuir (L), where $1 \text{ L}=1.33 \times 10^{-6}$ mbar s. Subsequent annealing to 700 K removed excess oxygen and produced the well-ordered $\text{Fe}(001)-p(1 \times 1)\text{O}$ surface, as reported in the literature.^{14–16} This was checked by monitoring the ratio of the O 510 eV Auger signal to the Fe 703 eV Auger signal as a function of oxygen exposure. A modulation technique was used to acquire the differential conductivity spectra directly by performing STS. In this case the bias voltage was modulated by a 30 mV ac signal at 6.5 kHz and changes in the differential conductivity detected with a lock-in amplifier.

The electronic and magnetic properties of the $\text{Fe}(001)-p(1 \times 1)\text{O}$ surface were calculated from first principles using a Green's-function multiple-scattering approach¹⁷ within density functional theory in the local spin-density approximation (LSDA). The method is specially designed for layered systems by an adequate treatment of the semi-infinite boundary conditions.¹⁸ To simulate scanning tunneling spectra we used the Tersoff-Hamann treatment for the tunneling current.¹⁹ In this approximation, the tunneling current is proportional to the LDOS of the surface at the tip position. In the present work, the LDOS was calculated from first principles from nonspherical potentials determined self-consistently for bulk, surface, and vacuum regions.

Oxygen adsorption onto iron surface induces strong atomic relaxations and modifications of the surface electronic states.^{10,20,21} Additionally, in an STM experiment the surface can experience deformations due to the tip or other experimental conditions. Therefore, it is important to account for these relaxations in first-principles calculations. In our simulations the atomic positions for the $\text{Fe}(001)-p(1 \times 1)\text{O}$ surface were determined with a semiempirical approach. In this approach we compared the LDOS, calculated in vacuum at 4 Å above the surface, with the experimental normalized differential conductance spectrum. Thereby we varied atomic positions within the first three layers to adjust the theoretical LDOS with the experimental results. In the following, whenever we refer to 4 Å above the surface, it means the distance

measured from the last plane of Fe atoms, both in the case of a clean $\text{Fe}(001)$ surface as for the $\text{Fe}(001)-p(1 \times 1)\text{O}$ surface. We started our simulations using structural information obtained from a dynamical LEED experiment.¹⁰ The resulting interlayer distances were found to be very close to the experiment of Jona *et al.*:¹⁰ 0.46 Å for O-Fe, 1.53 Å for the first, and 1.44 Å for the second Fe-Fe layers (bulk value 1.43 Å). Furthermore, we found a significant sensitivity of the LDOS of the vacuum layers to the surface deformations.

III. RESULTS AND DISCUSSION

Figure 1 shows a constant current STM topography of the clean $\text{Fe}(001)$ surface (a) and the same surface after exposure to 6 L oxygen and annealing at 700 K (b). Oxygen exposure induces already changes to the topography as can be seen from the kinks along the step edges in Fig. 1(b). The kinks indicate the onset of bulk oxidation. Atomic resolution was not achieved on the clean $\text{Fe}(001)$ surface in our experiment due to the relatively weak atomic corrugation of this surface.²² On the oxygen covered surface, however, atomic resolution was achieved as shown in Fig. 2(a). The atomically resolved STM images are consistent with the (1×1) pattern observed in LEED (not shown here).

It is generally not straightforward to identify individual adsorbates chemically in atomically resolved STM images since it is unclear whether the contrast is dominated by geometric or electronic structure effects. The fact that an adsorbed atom lies geometrically above the surface does not generally mean it appears as a protrusion in an STM topographic image. The question arises as to whether the bright protrusions in the atomically resolved images represent the position of the Fe or O atoms. Tersoff and Hamann^{19,23} showed that if one models the STM tip with a spherical wave and considers wave functions for the sample that decay exponentially into the vacuum while propagating freely along the surface plane, then for small bias voltages V , the tunneling current can be expressed as $I=VN(\mathbf{R},E_F)$, where $N(\mathbf{R},E_F)$ is the LDOS at the Fermi energy E_F of the sample at the position \mathbf{R} of the probe tip or equivalently, the charge per unit energy from surface states at E_F . Under constant current tunneling conditions, the STM tip is roughly expected to follow contours of constant LDOS several angstroms above the surface. These plots of the charge density within the surface-vacuum region would be representative for the actual STM image. In Fig. 2(b), such a plot obtained from our first-principles calculations at the Fermi level about 4 Å above the surface [top view of (100) plane], is shown. The charge density contours extend higher above the four-fold coordinated oxygen atoms (white spots), hence they appear as the bright protrusions in the atomically resolved STM images. This fact is as well proven by the examination of the equi-LDOS contours calculated on the (110) plane perpendicular to the surface [see the inset in Fig. 2(b)]; here the contour is taken for the charge density of $7 \times 10^{-5} e\text{Å}^{-3}$. The contour above the oxygen atoms is about 0.53 Å higher than above the iron atoms in agreement with the experimental corrugation of 0.1 Å in STM images. Thus, the bright spots in the STM topography image are identified with the oxygen

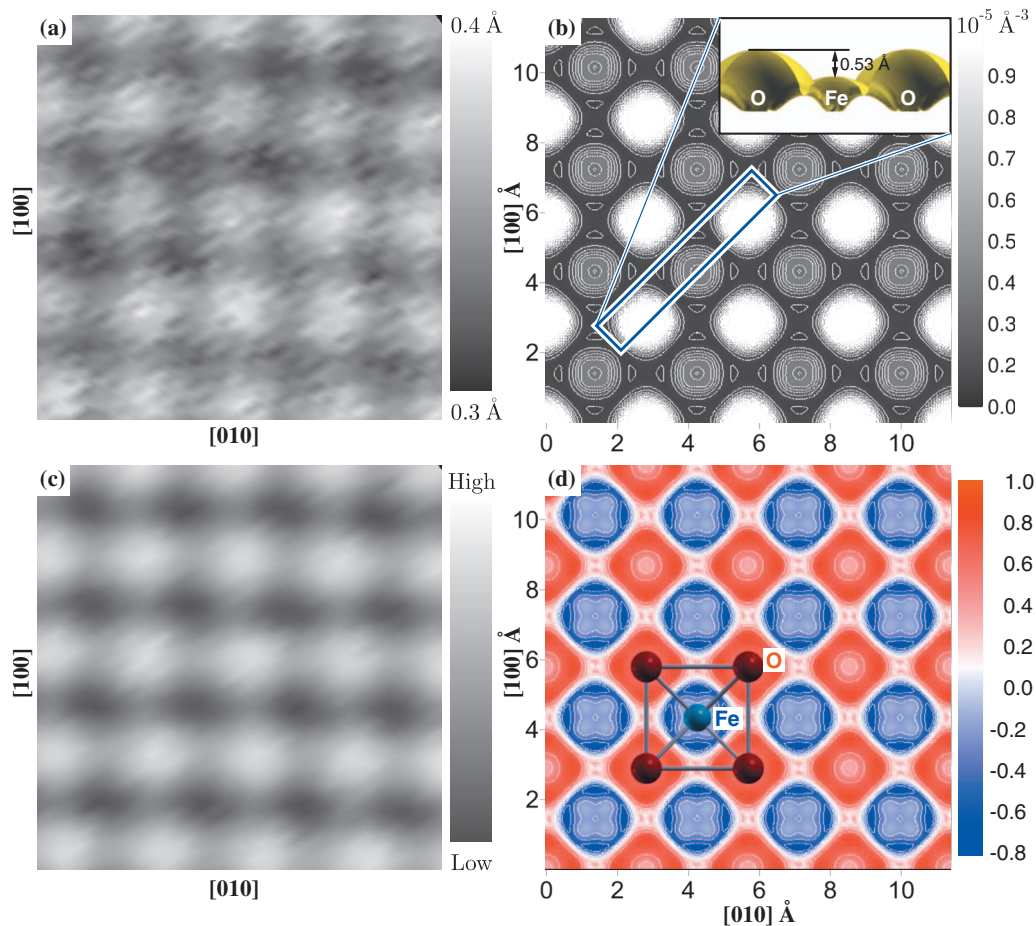


FIG. 2. (Color) (a) Atomically resolved topography of the Fe(001)- $p(1 \times 1)$ O surface. (b) Charge density at the Fermi level calculated in vacuum about 4 Å above the surface [top view of (001) plane]. Inset: equal-density contour of the charge density of $7 \times 10^{-5} e\text{Å}^{-3}$ calculated on the vertical (110) plane. (c) Spin image obtained simultaneously with the topography in (a) at 0.3 V sample bias. (d) Spin polarization at the Fermi level corresponding to the charge density presented in (b).

atoms while the dark spots reflect the underlying iron atoms.

According to the Tersoff-Hamann model, Sp-STM images of magnetic structures are reflected by the difference between tunneling currents for majority and minority spins and correspond to the local spin polarization.²⁴ The spin image obtained simultaneously with the topography is shown in Fig. 2(c). The bright spots are attributed to a large (positive) spin polarization while regions of low (negative) spin polarization appear dark. This spin image has the same periodicity as the topography with the maximum spin signal above the oxygen atoms, i.e., the spin polarization of the tunneling current has a maximum at the position of the oxygen atoms. This fact is confirmed by our first-principles simulations of the spin polarization. In Fig. 2(d) we show the spin polarization at Fermi level calculated in vacuum at 4 Å above the surface. The high and positive spin polarization (red color) is located mainly in positions above the oxygen atoms while the low spin polarization (blue color) is present in regions above the iron atoms. In the interstitial region above the iron positions, there is a negative spin polarization indicating large weight of minority spin states of iron. However, the full spin density integrated over all occupied electron states is prevalently positive, in excellent agreement with the predictions of Wu and Freeman²⁵ and Tsybmal *et al.*,²⁶ who found

that the full spin density at the surface is dominated by the positive cloud from the oxygen adsorption sites, which extend outwards into the vacuum.

In order to probe further the origin of the enhanced spin-dependent properties of this surface, we have studied changes in the LDOS caused by oxygen adsorption close to the Fermi level by means of STS obtained with nonmagnetic tungsten tips. The differential conductance spectra and the corresponding LDOS at 4 Å above the surface calculated from first principles are shown in Fig. 3. The dI/dV signal has been normalized with I/V to reduce the exponential background due to the voltage dependence of the tunneling probability.

Figure 3(a) displays the normalized differential conductance spectrum for the clean Fe(001) surface. A peak is seen at 0.15 V in agreement with Stroscio *et al.*²⁷ This peak corresponds to the well known minority surface state on Fe(001) which originates from unperturbed d orbitals extending into the vacuum. This peak as well as other features of the experimental data are reasonably well reproduced by our first-principles simulations [see Fig. 3(b)]. In our simulations the $d_{3z^2-r^2}$ resonance is found around 0.19 eV which is in excellent agreement with previous full-potential Korringa-Kohn-Rostoker (KKR) Green's-function calculations.²⁸ Figure 3(c)

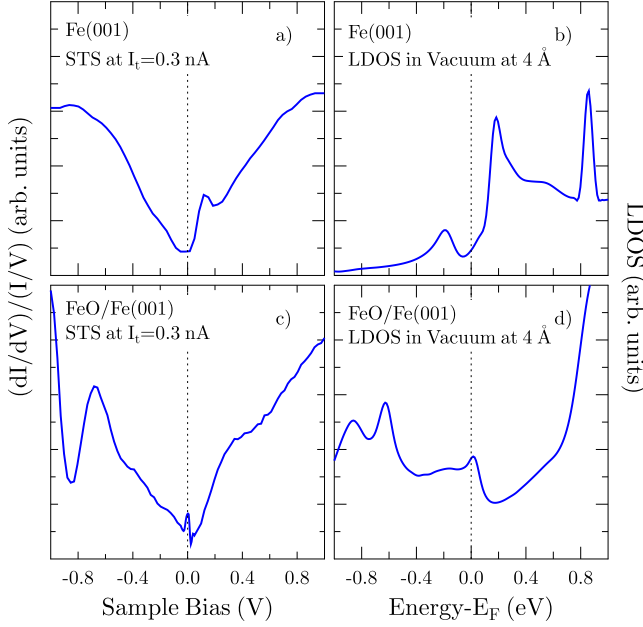


FIG. 3. (Color online) Normalized differential conductance spectra and corresponding spin averaged LDOS calculated at 4 Å above the surface for the clean [(a) and (b)] Fe(001) and [(c) and (d)] Fe(001)- $p(1 \times 1)$ O, respectively. The tip was held at 0.9 V and 0.3 nA, while the voltage was ramped between -0.9 and 0.9 V.

shows the differential conductance spectrum for the Fe(001)- $p(1 \times 1)$ O surface. Two peaks are observed at the Fermi level and at -0.7 V. A broader shoulder centered at 0.25 V is believed to be the minority surface state peak of the clean Fe(001) surface, which is shifted to higher energy and almost quenched.²⁹ These results are different from the measurements of Donati *et al.*⁸ since they are obtained at different experimental conditions. The calculated LDOS of the Fe(001)- $p(1 \times 1)$ O, estimated in vacuum at 4 Å above the surface, reproduces well the peak at the Fermi level and shows two other peaks at -0.62 and -0.81 eV [see Fig. 3(d)]. The peak at -0.62 eV can be associated with the experimental one at -0.7 V, while the second peak at -0.81 eV is not observed in the current experiment and is out of the measured voltage interval. Moreover, the broader shoulder observed at 0.25 V is not reproduced in our simulations. The discrepancy between theory and experiment can be explained by limitations of the Tersoff-Hamann model (neglect of the electronic structure of the tip) and the local density approximation, which fails to describe correctly excitations and electronic states in vacuum.

From atomically resolved spin-polarized STM images we obtained a spin contrast of Fe(001)- $p(1 \times 1)$ O surface. This contrast, which is a result of the difference in the spin-polarized tunneling current between O and Fe, shows strong dependence on the applied voltage from -1 to +1 V (see Fig. 4, black line). It is small and positive, with the maximum contrast at 0.1 V, decreases as the voltage increases, and is smaller for higher negative voltages. No change in sign of the contrast was observed within the voltage range in the experiment. To compare the experimental spin contrast with our first-principles simulations we estimated a differ-

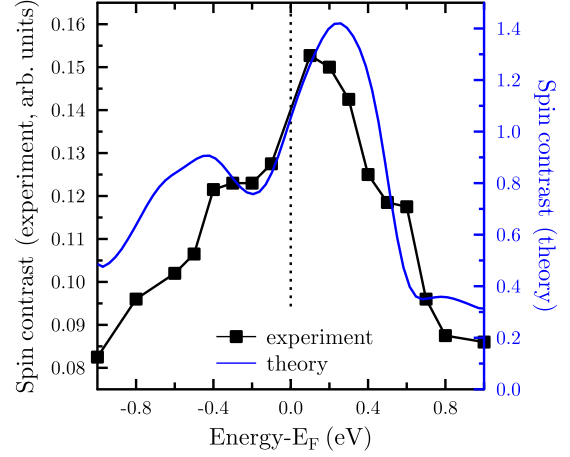


FIG. 4. (Color online) Spin contrast of Fe(001)- $p(1 \times 1)$ O surface: measured as a function of bias voltage from atomically resolved spin-polarized STM (black line) and calculated as a function of energy from the local density of state at 4 Å above the surface layer reflecting the STM experiment (blue line).

ence between the atomically resolved spin polarizations $P_O - P_{Fe}$ as a function of energy (Fig. 4, blue line). The polarization P_A of an atom A is defined as

$$P_A = \frac{n_A^\uparrow - n_A^\downarrow}{n_A^\uparrow + n_A^\downarrow}. \quad (1)$$

The spin and atomically resolved LDOS $n_A^{\uparrow(\downarrow)}$ was evaluated in vacuum within the area corresponding to a particular surface atom A at 4 Å above the sample. The simulated spin contrast shows a similar trend like the experimental one, except for the maximum which occurs at 0.23 eV. Moreover, the theoretical curve is broader than the experimental one. These deviations may be due to effects of the tip-spin polarization which is not taken properly into account in our simulations.

To elucidate the experimental results we performed a systematic comparison of electronic and magnetic properties of the clean Fe(001) and Fe(001)- $p(1 \times 1)$ O surfaces using our self-consistent KKR Green's-function method. The obtained spin-resolved LDOS and the corresponding magnetic moments of the surface and two subsurface layers are presented in Fig. 5. The results of our calculations are, in general, in good agreement with previous first-principles calculations for the clean Fe(001) and Fe(001)- $p(1 \times 1)$ O surfaces.^{3,25,26,28,30-32} Due to strong symmetry reduction, the d bands of the clean Fe(001) surface are more localized than in bulk. Furthermore, the bulk t_{2g} and e_g bands are split in the surface and subsurface layers, into d_{xy} , $d_{xz,yz}$, $d_{3z^2-r^2}$, and $d_{x^2-y^2}$ states, according to the reduced symmetry.³ In the majority spin channel, the surface d bands are almost fully occupied forming a quasi-half-metallic density of states,³³ while the minority $d_{3z^2-r^2}$ is shifted toward the occupied valence bands inducing thereby a strong negative spin polarization in the vicinity of the Fermi level. As a result, the surface magnetic moment is strongly enhanced and is about $2.98\mu_B$ in our calculations.

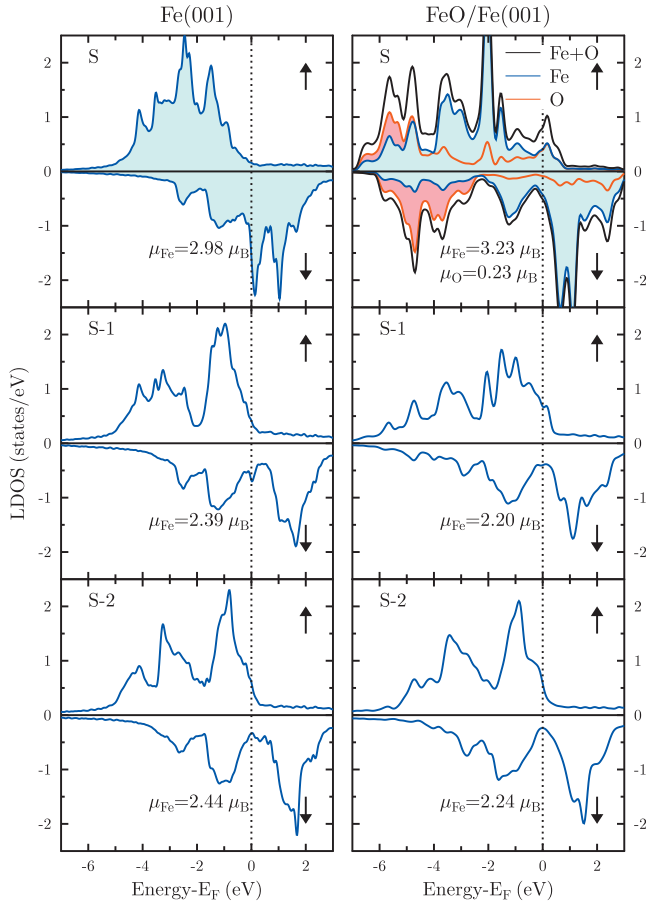


FIG. 5. (Color) Spin resolved densities of states of the surface (*s*) and two subsurface (*S-1*, *S-2*) layers for the clean Fe(001) (left) and Fe(001)-*p*(1×1)O (right). Top: black line represents total LDOS of the surface; blue line and shaded area represent the Fe LDOS; red line and shaded area represent the O LDOS.

The chemical bond with the oxygen in the Fe(001)-*p*(1×1)O surface leads to additional localization of the Fe *d* bands.³ Oxygen forms *p* bonding states below the *d* bands of Fe which are located around 5.5 eV below the Fermi level. Since the *d* bands are occupied differently in the majority and minority spin channels, the strong hybridization between O *p* and Fe *d* states induces a magnetic moment in oxygen which is about $0.23\mu_B$ according to our calculations and is in good agreement with the previous first-principles studies.^{3,25,26,32} Apart from the bonding levels, the oxygen forms a broad band of antibonding levels which are partially occupied and are extended up to 3 eV above the Fermi level. The bonding of these levels with Fe bands shifts a part of the *d* states in both spin channels away from the Fermi energy, increasing the magnetic moment of Fe up to $3.23\mu_B$ and inducing a large positive spin polarization at the Fermi level.^{3,26}

To explain the main features of our STS experiment, we analyzed the LDOS of the first vacuum layer, the surface, and subsurface layers within the energy range corresponding to the applied bias voltage, from -1 to 1 V. In case of the clean Fe(001) surface (left panel of Fig. 6), the spin-resolved LDOS of the vacuum layer shows some peaks only in the

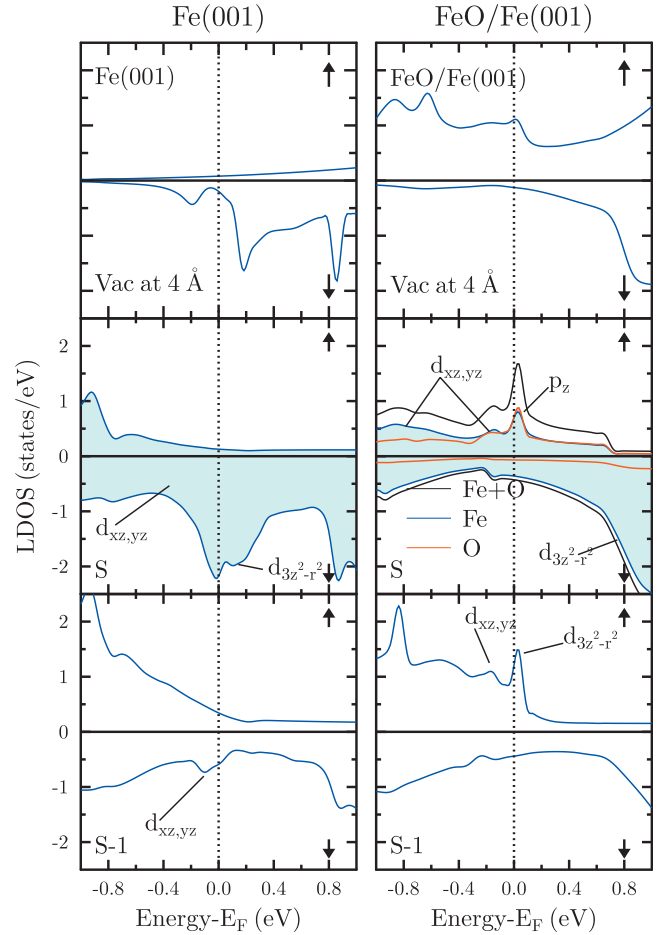


FIG. 6. (Color) Spin resolved densities of states of the vacuum (Vac), surface (*s*) and subsurface (*S-1*) layers for the clean Fe(001) (left) and Fe(001)-*p*(1×1)O (right) within the energy range corresponding to the applied bias voltage. Only selected states, which participate in the tunneling process, are indicated. Middle (right): black line represents total LDOS of the surface; blue line and shaded area represent the Fe LDOS; red line and shaded area represent the oxygen LDOS.

minority spin channel. The resonance at 0.19 eV above the Fermi level has $s-d_{3z^2-r^2}$ symmetry and reflects the corresponding *d* state of the clean Fe surface.²⁷ In case of oxidized Fe surface, this state is shifted away from the Fermi level toward unoccupied antibonding oxygen levels and is located around 1 eV above the Fermi energy (right panel of Fig. 6). Oppositely, in the majority spin channel the strong hybridization between Fe *d* and O *p* bands leads to the formation of states around -0.8 – -0.7 eV and at the Fermi level. The peaks around -0.8 – -0.7 eV can be identified with Fe $d_{xz,yz}$ states hybridized with O $p_{x,y}$ levels. The resonance at the Fermi level is associated with an O p_z state strongly hybridized with Fe d_{xy} bands of the surface layer and Fe $d_{3z^2-r^2}$ bands of the subsurface layer. Since d_{xy} states cannot be observed in STM experiment, we can conclude that the resonance at the Fermi level, observed in our STS experiment and reproduced in our simulations, is mainly originated from the O p_z state. In its turn this resonance arises due to a strong hybridization with Fe $d_{3z^2-r^2}$ state of the subsurface layer.

The origin of such a strong hybridization between top oxygen and iron subsurface layers lies in the crystalline structure of the Fe(001)- $p(1 \times 1)$ O surface. According to the LEED measurements of Jona and Markus¹⁰ and a recent first-principles structural optimization,²⁰ the O atoms occupy the fourfold hollow sites and have an adsorption height of about 0.45–0.48 Å. The resulting Fe–O bond lengths of 2.08 and 2.02 Å for the surface and subsurface Fe atoms are of the same order. Therefore, besides the strong O p and Fe d hybridization at the surface, there is a substantial chemical bond between O p_z and Fe $d_{3z^2-r^2}$ states from the subsurface layer.³

IV. CONCLUSION

We have presented a combined experimental and first-principles study on electronic and magnetic properties of Fe(001)- $p(1 \times 1)$ O surface. A well-ordered Fe(001)- $p(1 \times 1)$ O surface was prepared by exposing a clean Fe whisker to 6 L oxygen and annealing at 700 K. Our atomic scale spin-polarized STM measurements confirm the atomic registry in real space, which had been previously studied in reciprocal space by LEED. The oxygen atoms sit in the fourfold hollow sites on the surface and are imaged as protrusions

at these sites in atomically resolved STM. The atomically resolved spin image shows good agreement with the spin-density contour for the system obtained from our theoretical calculations, where the maximum spin signal is obtained above the oxygen sites. The oxygen absorption stabilizes ferromagnetism of the Fe(001) surface and induces positive spin polarization at the Fermi level. The differential conductance spectrum of the surface obtained from scanning tunneling spectroscopy identified features around -0.7 V and at the Fermi level. Our first-principles calculations reveal that the first feature results from a hybridization of the oxygen p_x, p_y orbitals with the iron $d_{x^2-y^2}$ states of the surface layer. The peak at the Fermi level has an O p_z character and is originated from a substantial chemical bond between O p_z and Fe $d_{3z^2-r^2}$ states from the subsurface layer.

ACKNOWLEDGMENTS

This work was supported by the *Sonderforschungsbereich* SFB 762, “Functionality of Oxide Interfaces.” We gratefully acknowledge H. L. Meyerheim and S. Ostanin for many stimulating discussions. The calculations were performed at the John von Neumann Institute in Jülich and Rechenzentrum Garching of the Max Planck Society (Germany).

-
- ¹A. Clarke, N. B. Brookes, P. D. Johnson, M. Weinert, B. Sinković, and N. V. Smith, *Phys. Rev. B* **41**, 9659 (1990).
²M. Getzlaff, J. Bansmann, and G. Schoenhense, *J. Magn. Magn. Mater.* **192**, 458 (1999).
³H. Huang and J. Hermanson, *Phys. Rev. B* **32**, 6312 (1985).
⁴P. D. Johnson, *J. Electron Spectrosc. Relat. Phenom.* **51**, 249 (1990).
⁵R. Bertacco, M. Merano, and F. Ciccacci, *Appl. Phys. Lett.* **72**, 2050 (1998).
⁶R. Bertacco and F. Ciccacci, *Phys. Rev. B* **59**, 4207 (1999).
⁷A. Winkelmann, D. Hartung, H. Engelhard, C.-T. Chiang, and J. Kirschner, *Rev. Sci. Instrum.* **79**, 083303 (2008).
⁸F. Donati *et al.*, *Phys. Rev. B* **79**, 195430 (2009).
⁹S. R. Chubb and W. E. Pickett, *Solid State Commun.* **62**, 19 (1987).
¹⁰F. P. Jona and P. M. Marcus, *Solid State Commun.* **64**, 667 (1987).
¹¹W. Wulfhekel and J. Kirschner, *Appl. Phys. Lett.* **75**, 1944 (1999).
¹²U. Schlickum, W. Wulfhekel, and J. Kirschner, *Appl. Phys. Lett.* **83**, 2016 (2003).
¹³W. Wulfhekel and J. Kirschner, *Annu. Rev. Mater. Res.* **37**, 69 (2007).
¹⁴K. O. Legg, F. P. Jona, D. W. Jepsen, and P. M. Marcus, *J. Phys. C* **8**, L492 (1975).
¹⁵C. Leygraf and S. Ekelund, *Surf. Sci.* **40**, 609 (1973).
¹⁶J.-P. Lu, M. R. Albert, S. T. Bernasek, and D. J. Dwyer, *Surf. Sci.* **215**, 348 (1989).
¹⁷M. Lüders, A. Ernst, W. M. Temmerman, Z. Szotek, and P. J. Durham, *J. Phys.: Condens. Matter* **13**, 8587 (2001).
¹⁸L. Szunyogh, B. Újfalussy, P. Weinberger, and J. Kollár, *Phys. Rev. B* **49**, 2721 (1994).
¹⁹J. Tersoff and D. R. Hamann, *Phys. Rev. Lett.* **50**, 1998 (1983).
²⁰P. Błoński, A. Kiejna, and J. Hafner, *Surf. Sci.* **590**, 88 (2005).
²¹S. S. Parihar, H. L. Meyerheim, K. Mohseni, S. Ostanin, A. Ernst, N. Jedrecy, R. Felici, and J. Kirschner, *Phys. Rev. B* **81**, 075428 (2010).
²²J. A. Stroscio and D. T. Pierce, *J. Vac. Sci. Technol. B* **12**, 1783 (1994).
²³J. Tersoff and D. R. Hamann, *Phys. Rev. B* **31**, 805 (1985).
²⁴S. Heinze, P. Kurz, D. Wortmann, G. Bihlmayer, and S. Blügel, *Appl. Phys. A: Mater. Sci. Process.* **75**, 25 (2002).
²⁵R. Wu and A. J. Freeman, *J. Magn. Magn. Mater.* **127**, 327 (1993).
²⁶E. Y. Tsymbal, I. I. Oleinik, and D. G. Pettifor, *J. Appl. Phys.* **87**, 5230 (2000).
²⁷J. A. Stroscio, D. T. Pierce, A. Davies, R. J. Celotta, and M. Weinert, *Phys. Rev. Lett.* **75**, 2960 (1995).
²⁸N. Papanikolaou, B. Nonas, S. Heinze, R. Zeller, and P. H. Dederichs, *Phys. Rev. B* **62**, 11118 (2000).
²⁹M. M. J. Bischoff, T. K. Yamada, C. M. Fang, R. A. de Groot, and H. van Kempen, *Phys. Rev. B* **68**, 045422 (2003).
³⁰C. S. Wang and A. J. Freeman, *Phys. Rev. B* **24**, 4364 (1981).
³¹S. Ohnishi, A. J. Freeman, and M. Weinert, *Phys. Rev. B* **28**, 6741 (1983).
³²R. Wu and A. J. Freeman, *Phys. Rev. Lett.* **69**, 2867 (1992).
³³W. Wulfhekel, A. Ernst, J. Henk, P. Bruno, J. Kirschner, F. Zavaliche, C. C. Kuo, and M.-T. Lin, *Phys. Rev. B* **72**, 212407 (2005).